AD_____

Award Number: W81XWH-07-1-0228

TITLE: Developing a Zebrafish Model of NF1 for Structure-Function Analysis and Identification of Modifier Genes

PRINCIPAL INVESTIGATOR: Jonathan A. Epstein, M.D.

CONTRACTING ORGANIZATION: University of Pennsylvania
Philadelphia, PA 19104

REPORT DATE: April 2009

TYPE OF REPORT: Annual

PREPARED FOR: U.S. Army Medical Research and Materiel Command
Fort Detrick, Maryland 21702-5012

REPORT DOCUMENTATION PAGE

Form Approved
OMB No. 0704-0188

1. REPORT DATE	2. REPORT TYPE	3. DATES COVERED
01-04-2009	Annual	1 APR 2008 - 31 MAR 2009

4. TITLE AND SUBTITLE

Developing a Zebrafish Model of NF1 for Structure-Function Analysis and Identification of Modifier Genes

5a. CONTRACT NUMBER

5b. GRANT NUMBER
W81XWH-07-1-0228

5c. PROGRAM ELEMENT NUMBER

6. AUTHOR(S)
Jonathan A. Epstein, M.D.

Email: epsteinj@mail.med.upenn.edu

5d. PROJECT NUMBER

5e. TASK NUMBER

5f. WORK UNIT NUMBER

7. PERFORMING ORGANIZATION NAME(S) AND ADDRESS(ES)

University of Pennsylvania
Philadelphia, PA 19104

8. PERFORMING ORGANIZATION REPORT NUMBER

9. SPONSORING / MONITORING AGENCY NAME(S) AND ADDRESS(ES)
U.S. Army Medical Research and Materiel Command
Fort Detrick, Maryland 21702-5012

10. SPONSOR/MONITOR'S ACRONYM(S)

11. SPONSOR/MONITOR'S REPORT NUMBER(S)

12. DISTRIBUTION / AVAILABILITY STATEMENT
Approved for Public Release; Distribution Unlimited

13. SUPPLEMENTARY NOTES

14. ABSTRACT

This progress report summarizes the second year of activity of this project focused on the identification and characterization of the zebrafish orthologs of the neurofibromatosis type 1 genes. This project involves work within the Epstein laboratory and collaboration with the laboratory of Dr. Thomas Look at the Dana Farber Cancer Institute as a sub-contract. This progress report summarized the collaborative work including results from both groups. During the first year, significant progress had been made in the isolation and characterization of two zebrafish orthologs, nf1a and nf1b. The genes have been sequenced and their expression patterns identified. The knockdown phenotypes have been characterized and include overgrowth of glia and cardiovascular abnormalities. During the second year, these knockdown phenotypes have been further characterized and stable fish lines harboring mutations in these genes have been generated and procured with additional work underway. Manuscripts have been submitted for publication and are presently being updated to address reviewers' comments.

15. SUBJECT TERMS
Zebrafish model of neurofibromatosis; Morpholino knockdown; Engineered zinc fingered nuclease; Tilling; Vascular Patterning;

16. SECURITY CLASSIFICATION OF:			17. LIMITATION OF ABSTRACT	18. NUMBER OF PAGES	19a. NAME OF RESPONSIBLE PERSON
a. REPORT	b. ABSTRACT	c. THIS PAGE			USAMRMC
U	U	U	UU	22	19b. TELEPHONE NUMBER *(include area code)*

Table of Contents

Introduction:

The purpose of this project is to develop a zebrafish model of type 1 neurofibromatosis. The reason that this animal model may be useful for the further understanding of this disease is that genetic and chemical screens will be possible in a high throughput format using this vertebrate system. In addition, structure-function analysis will be possible using the developing zebrafish model. Prior to this work, the *Nf1* genes in zebrafish had not been described or characterized. Zebrafish develop rapidly and are transparent during development allowing for easy visualization of many structures including the cardiovascular system. Genetic and chemical screens can be performed in high throughput modalities at relatively low cost. Emerging technologies allow for complex manipulation of gene expression. This project involves the collaboration of two established groups to coordinate efforts to take advantage of zebrafish as a model system for NF1.

Body of work:

Identification of *nf1a* and *nf1b*

We utilized a bioinformatics approach to identify the zebrafish orthologues of human *NF1*. Analysis of the seventh assembly (Zv7) of the zebrafish genome revealed two genes that are highly similar to *NF1* at the amino acid level (90.4% and 90.7% respectively), which we named *nf1a* and *nf1b*. These genes are highly related to one another (87.4% identical and 93.7% similar); *nf1a* and *nf1b* share similar genomic structures and each contains 57 exons. *nf1a* is located on chromosome 15 (Figure 1A) and predicts a 311 kD protein composed of 2755 amino acids while *nf1b* is located on chromosome 10 (Figure 1B) and predicts a 310 kD protein composed of 2747 amino acids.

***nf1a* and *nf1b* are broadly expressed early and become restricted to the nervous system during later embryogenesis.**

We searched the public database for zebrafish Expressed Sequence Tag (EST) clones using the sequences identified from Ensembl and found many ESTs spanning different regions of the *nf1a* and *nf1b* coding sequences, indicating that both genes are expressed. Among them, we obtained one EST clone for each gene, in order to evaluate the expression of *nf1a* and *nf1b* during development (see Materials and Methods). The expression of *nf1a* and *nf1b* throughout early blastula stages demonstrates the maternal contribution of these genes (Fig. 2A, 2F), and ubiquitous expression throughout the embryo continued up to 24 hours post fertilization (hpf), with levels being highest in the head (Fig. 2B, 2G). By 2 days post fertilization (dpf), *nf1a* expression remained high in the brain (Fig. 2C-E), as demonstrated in transverse sections along the diencephalon and tegmentum (Fig. 2N), unlike the expression of *nf1b*, which rapidly decreased with time (Fig. 2H-J). Importantly, both *nf1a* and *nf1b* continued to be expressed, albeit weakly, throughout the spinal cord during later stages (Fig. 2D-E for *nf1a*; 2I-J for *nf1b*; K and L for higher magnifications). *nf1a* expression in the transverse section through the embryonic trunk shows expression in the cytoplasm of both neurons and glia (arrowheads in Fig. 2M) and is clearly evident in the axonal tracts of the spinal cord (arrows in Fig. 2M). *nf1b* expression shows a similar pattern of expression in the spinal cord but is much weaker (data not shown). In addition, strong expression of *nf1a*, but not *nf1b*, is detected in the retina during later stages of development (Fig 2D-E, 2I-J). Transverse sections show that *nf1a* is enriched in the ganglion cell layer and inner nuclear layer of the retina (rgc and inl in Fig. 2O), and *nf1b* is weakly expressed in the gut (Fig. 2P) supporting the possibility that these genes have distinct functional roles in these other tissues. However, during

these late embryonic stages, the principal expression domains of *nf1a* and *nf1b* reside in the central nervous system (CNS).

The number of OPCs is increased upon Nf1 knockdown

In order to test the role of *nf1a* and *nf1b* in zebrafish oligodendrocyte development, we used the morpholino knockdown of each gene in the *olig2-EGFP* transgenic zebrafish line bred into both wild type and *p53 -/-* backgrounds. The *olig2-EGFP* transgenic line expresses EGFP in OPCs throughout oligodendrocyte development. The *olig2-EGFP* transgenic line in the *p53* mutant background was used to circumvent non-specific effects due to morpholino toxicity. To knockdown Nf1 function, we designed and injected *nf1*-specific splice-blocking morpholinos (two were generated against *nf1a* and one for *nf1b*) into the *olig2-EGFP* transgenic zebrafish lines. The efficiency of the morpholinos was confirmed by RT-PCR at 3 dpf, and the production of aberrant bands upon morpholino knockdown demonstrated inappropriate splicing (arrowheads in Fig. 3A; morpholinos *nf1a*-e7 and *nf1b*-e4 are shown). The fact that *nf1a*-e7 injection led to several aberrant bands suggested that there were multiple cryptic donor sites within the exon 7 that can lead to splicing of *nf1a*. These aberrant bands were sequenced and confirmed to contain deletions of the targeted exons or insertions of additional introns that resulted in frame-shifts in coding sequence leading to early transcript termination (data not shown).

In *olig2-EGFP* transgenic zebrafish, a subset of GFP+ OPCs that are born in the ventral spinal cord migrate dorsally and differentiate into oligodendrocytes (brackets in Fig. 3B, 3F, 3J), while a second GFP+ OPC subpopulation remains in the ventral spinal cord, intermingled with *olig2-EGFP* + motoneurons and interneurons. When *nf1a* and *nf1b* were knocked down using morpholinos, we consistently found an increased number of dorsally positioned OPCs at 3 dpf (Fig. 3B, 3F, 3J). The most dramatic OPC increase relative to control was observed when both the *nf1a* and *nf1b* genes were knocked down together in the *p53 -/-* background (Fig. 3J), although increases were also observed in individual *nf1* gene knock-downs (Fig. 3F, 3N). These results indicate that both *nf1* genes normally regulate the numbers of OPCs, and that *nf1* knockdown results in an increased number of dorsally positioned OPCs.

This phenotype was extended to the evaluation of ventrally positioned OPCs by co-immunostaining with an anti-sox10 antibody that labels OPCs, but not *olig2-EGFP* + motoneurons and interneurons that are located in the spinal cord at this stage. The increased number of *olig2-EGFP* +; sox10+ OPCs in *nf1a* and 1b morphants was evident in transverse sections of the spinal cord (Fig. 3K-M, compared to 3G-I). The mean number of OPCs was determined for *nf1a+nf1b* morphants and control embryos by counting OPCs in immunostained transverse sections. The *nf1* morphants were found to have 36% more OPCs than control *p53 -/-* embryos (9.0 vs. 6.6 respectively, n=23 and 26, $p<0.0001$; Fig. 3N). These findings document that one of the functions of *nf1* is to negatively regulate the number of OPCs during development. Although the OPCs in *nf1* morphants exhibit signs of increased motility and migration (see below), the observed increase in OPCs is not due to an aberrant dorsal migration of OPCs that normally would remain the ventral spinal cord. The increase in OPC numbers was observed in both migrating and non-migrating OPC populations when they were assessed separately (n=11, $p<0.05$). Also, while there is a slightly higher increase in OPCs in the p53 mutant background, presumably due to the survival of cells that would otherwise succumb to morpholino toxicity, it is important to note that significant increases in OPCs were also observed in the wild type background (Fig. 3N).

***nf1* loss specifically affects OPCs from the pMN of the ventral spinal cord**

To address whether the loss of *nf1* also affected *olig2-EGFP*-positive motoneuron derivatives forming in the pMN of the ventral spinal cord, we examined the expression of *islet 1* which is expressed

in primary/secondary motor neurons, interneurons, and sensory neurons of the spinal cord, and *zn-5* which is a marker for developing secondary motoneurons. Quantification of cell numbers using anit-isl and zn5 antibodies failed to indicate significant differences in cells expressing either of these markers in *nf1a+b* knockdown embryos compared to control s (Fig. 4 F vs B; N vs J; Q and R) . In addition, *nf1a+b* loss did not affect the overall size or shape of developing secondary motoneurons (Fig 4 N vs J). These results suggest that *nf1* knockdown acts specifically on the oligodendrocyte lineage, while the neuronal lineages from the pMN domain, such as motoneurons, are not affected.

***nf1* loss promotes OPC motility**

In order to examine the cellular behavior of OPCs following *nf1* knockdown, we carried out live time-lapse imaging *in vivo.* We monitored the *olig2-EGFP* transgenic animals for 12 hours, beginning at 60 hpf when OPCs are actively migrating away from the ventral spinal cord. Compared to OPCs in uninjected control p53 -/- animals, more OPCs in the *nf1a+1b*-knockdown *p53-/-* embryo were observed to enter the dorsal spinal cord (Fig. 5A, B), consistent with our observations in fixed sections (Fig. 3). The time-lapse study also revealed that the motility of *nf1a+1b*-morphant OPCs is enhanced (Fig. 5E). When the velocity of individual migrating OPCs was measured based on the total distance traversed over time (μm/5 minute), a 36% increase was observed upon *nf1* knockdown (0.2686 vs. 0.3667 μm/5 min; $p<0.005$; Fig. 5E). *nf1a+1b*-knockdown OPCs migrate further on average in the dorsal direction than control OPCs. They also show greater tangential movement, presumably due to their increased motility, but there is no net migration in either the rostral or caudal directions as shown by the individual migratory traces (Fig. 5 C and D). Therefore, *nf1* loss leads to an enhancement of motility in OPCs, a phenotype that has not been previously described.

***nf1* loss does not activate Ras signaling pathways in OPCs**

The best-known function of Nf1 is to act as a Ras-GAP to down-regulate Ras signaling through its downstream pathways. To investigate the effect of *nf1* loss on these pathways we evaluated the status of 1) phosphorylated ERK1/2, a downstream target of the Ras/Raf pathway and 2) phosphorylated ribosomal protein S6, a downstream target of the PI3 Kinase pathway. At 3 dpf, when the increased OPC numbers were evident, and more cells in transverse sections of the spinal cord *nf1a+1b*-knockdown embryos were labeled with a phospho-ERK1/2 antibody than in controls, indicating more cells with ERK activation. This is consistent with Nf1's role as a suppressor of signaling through the RAS/MAPK pathway (Fig. 6). However, we were surprised to find that the phospho-ERK1/2-positive cells in the dorsal spinal cord did not correspond to GFP-positive OPCs in either control or *nf1*-knockdown conditions. Thus, although the RAS/MAPK pathway was significantly activated in surrounding neurons, there was not a detectable increase in activity in the OPCs themselves. We also examined Akt/mTOR pathway activation and found that while phospho-S6-positive cells were detected, *nf1* loss did not cause significant changes in the numbers of phospho-S6-positive cells in the dorsal spinal cord, and GFP-positive OPCs labeled weakly if at all .

Morpholino knockdown of nf1a and nf1b results in cardiovascular defects

nf1a and *nf1b* morphant embryos also displayed gross abnormalities of cardiovascular development appreciable to the blinded observer by 48 hpf (Fig. 7). For example, 2 ng of an *nf1a* translation-blocking MO produced cardiac defects in 75% of injected embryos at 48 hpf, while only 5% of embryos injected with a control MO (containing 5 altered nucleotides) showed defects when assessed by a blinded observer. Morphant embryos frequently displayed a "to-and-fro" movement of blood within the heart. That is, blood was seen to move back and forth from atrium to ventricle, suggesting a

malfunctioning atrio-ventricular valve. In addition, we observed pooling of blood in the common cardinal vein and a paucity of blood flow along the dorsal aorta and posterior cardinal vein. Valvular insufficiency and reduced blood flow were not appreciated in control morphants or wild type embryos. Overall development of the embryos was relatively preserved through the first 3 days of development despite these cardiac defects. Histological analysis revealed a thinned ventricular myocardium and large pericardial effusions in MO-treated embryos. Gross morphological analysis also showed an increased incidence of pericardial effusions at 48 hpf, reflecting cardiac dysfunction, in *nf1a* and *nf1b* morhpants when compared with controls (Fig. 7). Non-specific toxicity arising from MO exposure as a cause of the observed cardiovascular defects was unlikely as unrelated control or scrambled MOs failed to produce similar levels of abnormalities, defects were observed even at low doses of specific MOs, and similar defects were observed with several unrelated but specific MOs directed against *nf1a* and *nf1b*. In addition, injection of specific MOs in p53 mutant embryos also produced similar cardiovascular defects, and off-target effects due to MO exposure is known to be at least partially mediated through p53 activation. Defects in cardiac valve morphogenesis and a thinning of the ventricular myocardium are also seen in *Nf1*-deficient murine embryos.

We performed knockdown experiments using zebrafish embryos in which endothelial cells are marked by expression of a cytoplasmic enhanced green fluorescent protein (EGFP) in order to allow for a more detailed analysis of vascular development. Dramatic abnormalities of vascular patterning in the intersomitic vessels of morphant embryos were present at 48 and 72 hpf (Fig. 8). In *nf1a* MO treated embryos, the leading edge of the sprouting vessels displayed claw-like projections at 48 hpf (Fig. 8C) and failed to pattern normally such that the dorsal longitudinal anastomotic vessel (DLAV) did not form or developed only in a rudimentary fashion (Fig. 8F). This occurred in embryos that were otherwise normal in overall size and maturity. Vascular pattering defects did not appear to correlate directly with cardiac defects, as we observed embryos with vascular abnormalities that did not display pericardial effusion or valvular insufficiency as assessed by a “to-and-fro” movement of blood within the heart. Blood flow within the dorsal aorta appeared intact in these embryos.

At earlier time-points, we assessed vascular defects caused by *nf1a* and *nf1b* knockdown in zebrafish embryos expressing a nuclear-localized EGFP in endothelial cells. Morphant embryos displayed a complete (Fig. 9A4) or partial absence of intersomitic vessels emanating from the dorsal aorta at 24 hpf when compared with stage-matched controls (Fig. 9A3). Overall morphology of morphant and control embryos appeared equivalent (Fig. 9A1-2) ruling out non-specific developmental delay. These defects were apparent following MO-mediated knockdown of *nf1a* or *nf1b* while knockdown of both together had an additive effect (Fig. 9B). Again, similar defects were observed with several unrelated but specific MOs directed against *nf1a* and *nf1b* (Fig. 10). Our analysis of morphant embryos at 24 hpf also revealed a caudal vessel defect. Morphant embryos displayed a cystic expansion in the region of the caudal artery and vein (Fig. 10B2) when compared with controls (Fig. 10B1). Identity of the expanded tissue as vascular was confirmed by expression of EGFP (Fig. 10B3-4) and the presence of red blood cells in the expanded region. This defect was present following knockdown of either *nf1a* or *nf1b* (Fig. 10C).

Additional confirmation of the role of *nf1a* in vascular development derives from studies using a genetic background sensitized to vascular insult. Flt4 is the zebrafish orthologue of VEGF receptor-3, and previous studies have employed MOs directed against *flt4* to investigate genetic interactions during zebrafish artery development. Additionally, *flt4* morphant zebrafish embryos display variable defects in segmental artery formation reminiscent of those identified in our *nf1* morphants. As *flt4* expression is restricted to endothelial cells, combined *nf1a* and *flt4* knockdown would be expected to reveal genetic interactions that are preferential to the vasculature. Endothelial-GFP expressing embryos were injected

with *flt4* MO alone and in combination with a MO directed against *nf1a*, and morphant embryos were assessed at 24 and 48 hpf. At the low doses of MOs used, 85% of *flt4*/*nf1a* compound morphants displayed abnormal vascular shunts at 48 hpf as compared to only 4-8% of individual *flt4* or *nf1a* morphants (Figure 9C). This defect was not apparent in control morphants.

Zebrafish *nf1a* and *nf1b* mutant lines

A ciritical part of our proposal involves the generation of stable zebrafish lines carrying mutations in *nf1a* and *nf1b*. These animals will verify our morpholino studies and be able to extend our analysis beyond transient assays. Furthermore, planned future studies include chemical and genetic screen strategies based on these animals that can contribute to therapeutic development. Through collaborative efforts we have used a reverse genetics technology called TILLING (Target Induced Local Lesions In Genomes) and found several *nf1a* missense mutant alleles and one nonsense mutant line in the *nf1a* gene (Fig. 11A and B). A second mutagenesis strategy based on retroviral insertion identified a single mutant line affecting the *nf1b* locus in the intron between exon 1 and 2 (Fig. 11B). These *nf1a* and *nf1b* mutant alleles have recently been recovered in our laboratory and being currently being tested for potential defects in oligodendrocyte and cardiovascular development.

Most recently, a new tool was developed allowing targeted gene-specific mutagenesis using Zinger Finger Nuclease (ZFN) technology in the zebrafish research field[28, 29]. Briefly, ZFN is an artificial nuclease designed to bind specific nucleotide sequences in a zinc finger-based domain and induced to cleave double strand DNA near the target sequence. Non-homologous end-joining repair results in small deletions or insertions in the gene of interest. We designed several ZFNs that can induce mutations in the specific sequences of the *nf1a* and *nf1b* genes and obtained three frame-shift mutations (*nf1a*^{D8}, *nf1a*^{D53} and *nf1a*^{D59}) and one in-frame insertion mutation (*nf1a*$^{+33/D8}$) in exon 25 of *nf1a* and an in-frame deletion mutation (*nf1b*^{D39}) in exon 17 of *nf1b*. Because the GRD domain in *nf1a* and *nf1b* spans exon 26 and exon 27, we expect that three frame-shift mutant alleles for *nf1a* should lack GAP activity. Our initial preliminary study examining oligodendrocyte development in one of these lines is very promising. We have bred the mutant carrying an 8bp deletion in exon 25 of *nf1a* (*nf1a*^{D8}) to the *olig2:gfp* transgenic line. The homozygous *nf1a*^{D8} mutant embryos appear morphologically normal and survive through two weeks of age indicating that they may be viable through adulthood. Importantly, we observed increased number of GFP^{+} OLCs in *nf1a*$^{D8/D8}$;*Tg(olig2:gfp)* mutant embryos when compared to wild-type or heterozygous *nf1a*^{D8} embryos (Fig. 12). We have also assayed oligdendrocyte development in the *nf1b* in-frame mutant, however no defects or differences in oligodendrocyte development have been detected thus far (data not shown). We are also just beginning to use a modified ZFN strategy that is reported to have improved efficacy, and we are employing this approach to further insure our obtaining stable mutants in the *nf1b* gene.

In summary

- The number of OPCs in the spinal cord are increased upon transient knockdown of nf1a and nf1b
- Phospho MAP kinase pathway may not be responsible for the OPC increase or be required non-cell autonomously
- Cardiac and vascular defects in *nf1a* and *nf1b* knockdown fish
- Several putative mutants for *nf1a* and *nf1b* have been identified and validated

Materials and Methods

1. **Immunohistochemistry** Fixed embryos were embedded in sucrose/agar mix and cryosectioned using cryostat machine with 14μm thick. Sections were incubated with the primary

antibodies (sox10, 1:5,000; GFP, 1:500, pMAPK, 1:200, pH3, 1:200) and Alexa 568 or 633 secondary antibodies.

2. **Whole mount in situ hybridization** Fixed embryos were permeabilized with proteinase K treatment (10ug/ml) with various incubation time depending on the stages of embryos, which then were incubated with DIG-labeled antisense RNA probes and visualized using alkaline phosphatase-conjugated anti-DIG antibody in color substrates.

3. **RT-PCR** cDNA for RT-PCR was made by reverse transcribing RNA prepared from morpholino (MO) injected embryos using Trizol, and PCR was performed to detect potential aberrant splicing. The triplicates of the same cDNA were used for the quantitative PCR to measure the knockdown by nf1b-e4 with beta-actin as baseline control.

4. **Confocal imaging** Zeiss LSM 510 META confocal microscope at Harvard Neurodiscovery imaging program was used for capturing confocal images of olig2-EGFP and other antibody staining in zebrafish spinal cord with 1-3μm optical sections.

5. **Counting OPCs and statistical analysis** Three sections of the spinal cord at the approximately similar anterior-posterior level from individual embryos (eight to ten embryos) were chosen for counting all of the GFP+/sox10+ cells within the section. Individual t-test were performed to test the significant differences in the number of GFP+/sox10+ cells in the spinal cord using Prism software.

6. **TUNEL** Chemicon ApopTag Red In Situ Apoptosis Detection Kit (S7165) was used for TUNEL staining. The protocol for cryosections in the munual was followed with minor modifications.

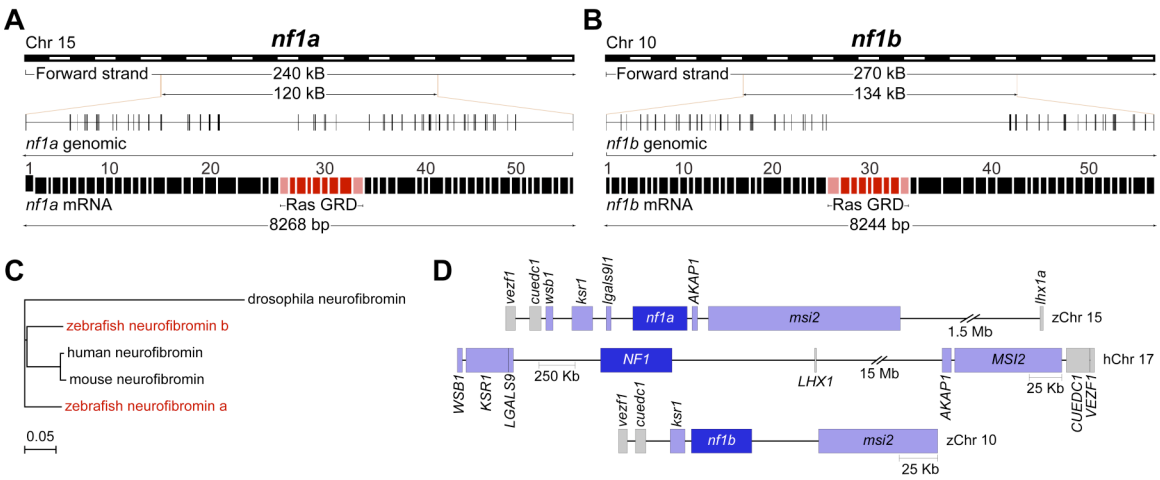

Fig. 1. **Zebrafish have two orthologues of human *NF1*.**
(**A**, **B**) Genomic and mRNA structures of the two orthologous zebrafish genes corresponding to human *NF1*. (**C**) Phylogenetic comparison of zebrafish, human, mouse, and Drosophila neurofibromin. (**D**) Analysis of syntenic relationships between human chromosome 17 (*NF1)* and zebrafish chromosomes 15 (*nf1a*), and 10 (*nf1b*). Both genes are flanked by upstream genes encoding WD repeat and SOCS box-containing 1 (WSB1), Kinase suppressor of Ras 1 (KSR1), and Galectin-9 (LGALS9) and downstream genes encoding A kinase anchor protein 1 (AKAP1) and RNA-binding protein Musashi homolog 2 (MSI2). Relative genomic positions are to scale as indicated.

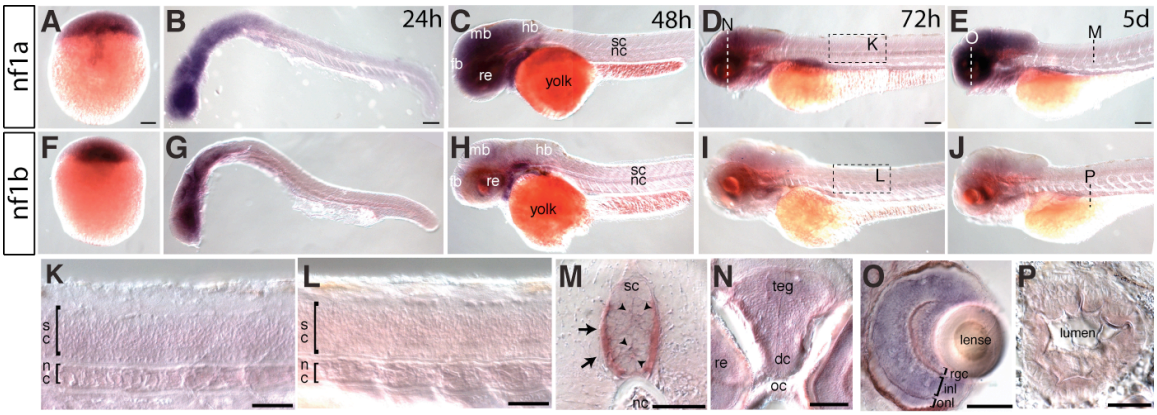

Fig. 2. The expression of *nf1a* and *nf1b* during embryogenesis by whole mount in situ hybridization.

nf1a expression: panels A-E, K, M, N, O. *nf1b* expression: panels F-J, P. A, F, one cell stage; B, G, 24hpf; C, H, 48hpf; D, I, 3dpf; E, J, 5dpf. **(A-E)** *nf1a* RNA is maternally supplied and expressed strongly throughout the embryo. Expression remains strong in the brain as development proceeds. **(F-J)** *nf1b* RNA is also maternally provided and expressed broadly at a high level during early embryogenesis, but its expression drops to low levels in the whole embryo after 2dpf. **(K, L)** At 3dpf, both *nf1a* and *nf1b* expression is weaker and becomes restricted to the spinal cord. **(M)** Transverse section of the spinal cord hybridized with the *nf1a* probe at 3dpf. Expression is cytoplasmic in neurons and glial cells (arrowheads), and axon tracts (arrows). **(N)** Expression of *nf1a* in a transverse section through a 3dpf-old embryo at the level of the optic chiasm (oc), showing broad expression in the diencephalon (dc) and the tegmentum (tg). **(O)** Transverse section of a 5dpf-old embryo retina hybridized with *nf1a*, showing strong expression in the retinal ganglion cells (rgc) and inner nuclear layer (inl). onl, outer nuclear layer. **(P)** *nf1a* and *nf1b* are also expressed outside the CNS. *nf1b* expression in a cross section through the gut at 5dpf is shown. fb, forebrain; mb, midbrain; hb, hindbrain; sc, spinal cord; nc, notochord. Scale bars in A-E = 100µm; K, L, N, O = 50µm; M, P = 25µm.

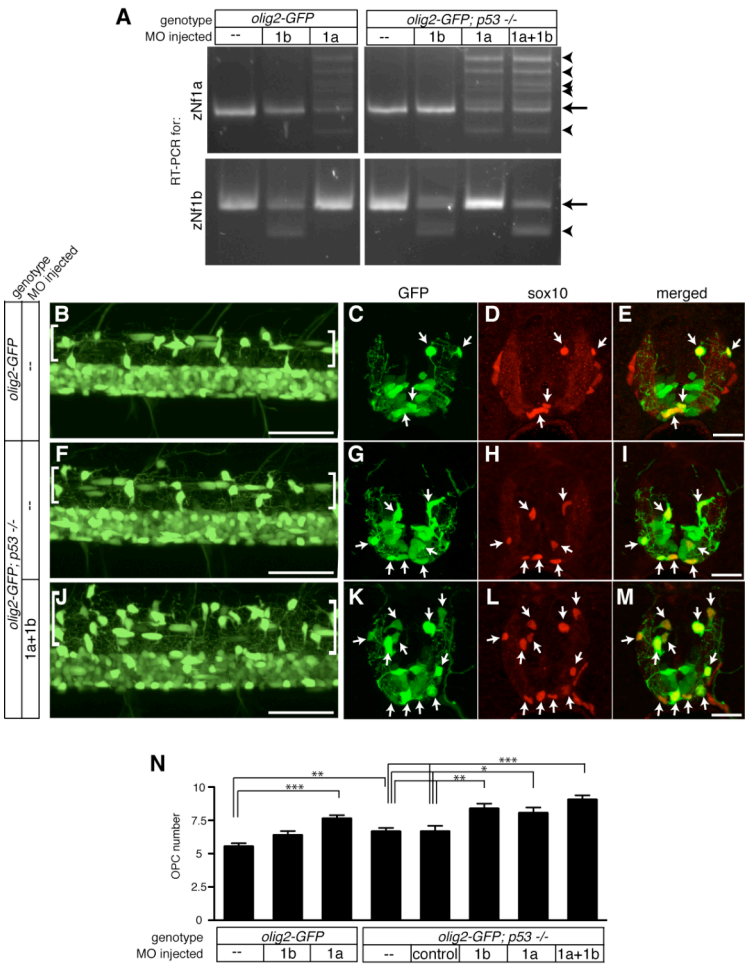

Fig. 3. The knockdown of *nf1a* and *nf1b* leads to increased numbers of OPCs.
(A) RT-PCR assays following the injection of *nf1a*-e7 and *nf1b*-e4 morpholinos individually or in combination into *olig2-EGFP* or *olig2-EGFP*;*p53-/-* embryos at 3dpf. The table above the picture denotes the injected morpholinos. Morpholino injections induce aberrant splicing resulting in the production of abnormal bands indicated by arrowheads while the arrows indicate wild type bands. **(B-E)** Uninjected *olig2-EGFP* transgenic zebrafish. **(F-I)** Control morpholino injected *olig2-EGFP*; *p53-/-* embryo. **(J-M)** *olig2-EGFP*; *p53-/-* injected with *nf1a* and *nf1b* morpholinos. **(B, F, J)** Projected confocal images show a lateral view of the spinal cord in live transgenic animals at 3dpf. The number of OPCs is increased upon morpholino injection (J), compared to uninjected or control morphants (B, F). **(C-E, G-I, K-M)** Transverse sections through the spinal cord of embryos at 3dpf, labeling GFP (green) and sox10 (red), to specifically visualize OPCs (arrows). The number of GFP+/sox10+ OPCs in morphant embryos is increased compared to controls, consistent with the lateral views (B, F, J), and confirms that OPCs in both the dorsal (migrating) and ventral (nonmigrating) spinal cord, increase in numbers. **(N)** Statistical analysis of averaged numbers of GFP+/sox10+ cells per section in *nf1a* (1a) or *nf1b* (1b) alone or in combination at 3pdf. Error bar indicates SEM, asterisks indicate statistical significance.

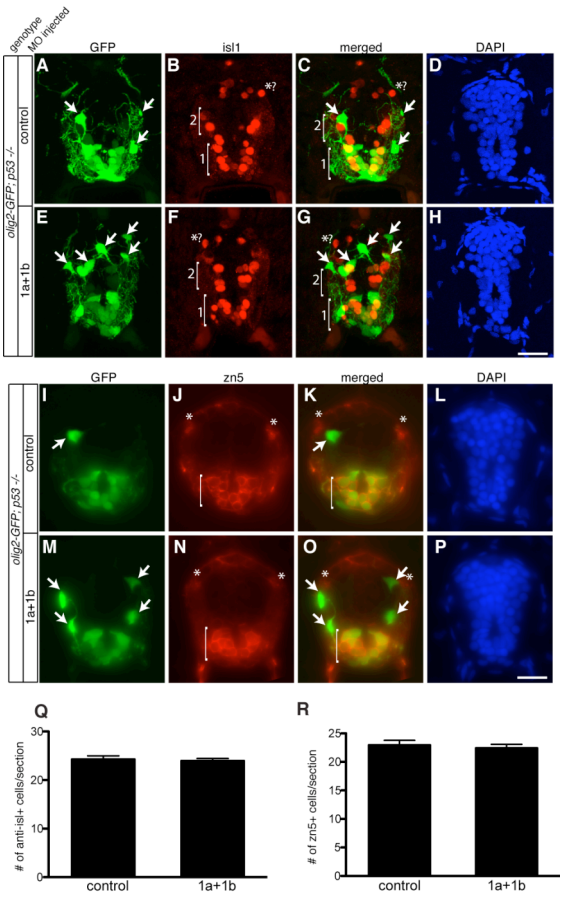

Fig. 4. Spinal cord neurons are not affected by Nf1 loss.
(A-D, I-L) *olig2-EGFP*;*p53-/-* embryos injected with the control morpholino. (E-H, M-P) An *olig2-EGFP*; *p53-/-* embryo injected with *nf1a* and *nf1b* morpholinos. **(A-H)** Projected confocal images of transverse sections labeled with the anti-*isl* antibody show subsets of primary/secondary motor neurons (bracket 1), interneurons (bracket 2), and sensory neurons (asterisk with a question mark). The number and morphology of anti-*isl*-positive cells appears to be unaffected upon nf1 knockdown. Green, *olig2*-GFP; red, anti-*isl*; blue, DAPI. Arrows in A, C, E, G, dorsal OPCs. **(I-P)** Fluorescence images of transverse sections labeled with the zn5 antibody showing secondary motor neurons. The number and morphology of zn-5-positive cells appears to be unaffected upon nf1 knockdown. Statistic analyses of the numbers of anti-isl1 (Q) or zn5 (R) show no significant differences (from 15 sections). Green, *olig2*-GFP; red, zn5; blue, DAPI. Arrows in I, K, M, O indicate dorsal OPCs; asterisks in J, K, N, O indicate the dorsal lateral fasciculus; brackets in J, K, N, O indicate secondary motoneurons. Scale bar = 20μm.

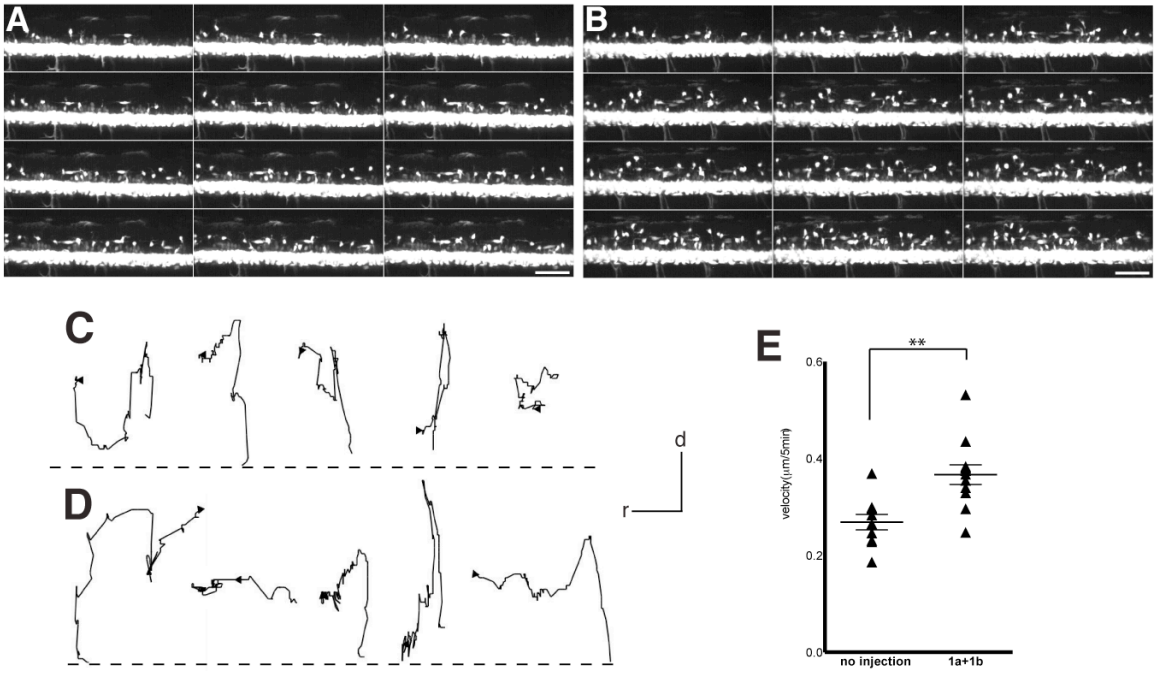

Fig. 5. nf1 loss enhances the motility of OPCs

(A, C) An uninjected *olig2-EGFP*; *p53-/-* control embryo; (B, D) An *olig2-EGFP*; *p53-/-* embryo injected with *nf1a* and *nf1b* morpholinos. **(A, B)** Montages of 12 hour time lapse images from 60hpf to 72hpf, showing the movements of OPCs every hour. Original images were taken every five minutes. For the complete movies, refer to Supplementary video 1. Compared to the uninjected control, OPCs with nf1 loss generally migrate at a higher velocity. **(C, D)** Cell migration paths are shown for OPCs that exhibited the highest calculated velocities. In either condition, their migration patterns appeared stochastic. Arrowheads indicate the end point of the cell's migration. Top, dorsal; left, rostral. **(E)** Graph showing the migration velocity of OPCs with or without Nf1 loss. Each triangle represents the velocities of ten individual OPC cells demonstrating the highest motility. n=10 for uninjected control embryos, n=12 for *nf1a*+1b morphant embryos. Scale bars in A, B = 25μm. Scale bars in C, D, X axis = 10μm, Y axis = 5μm.

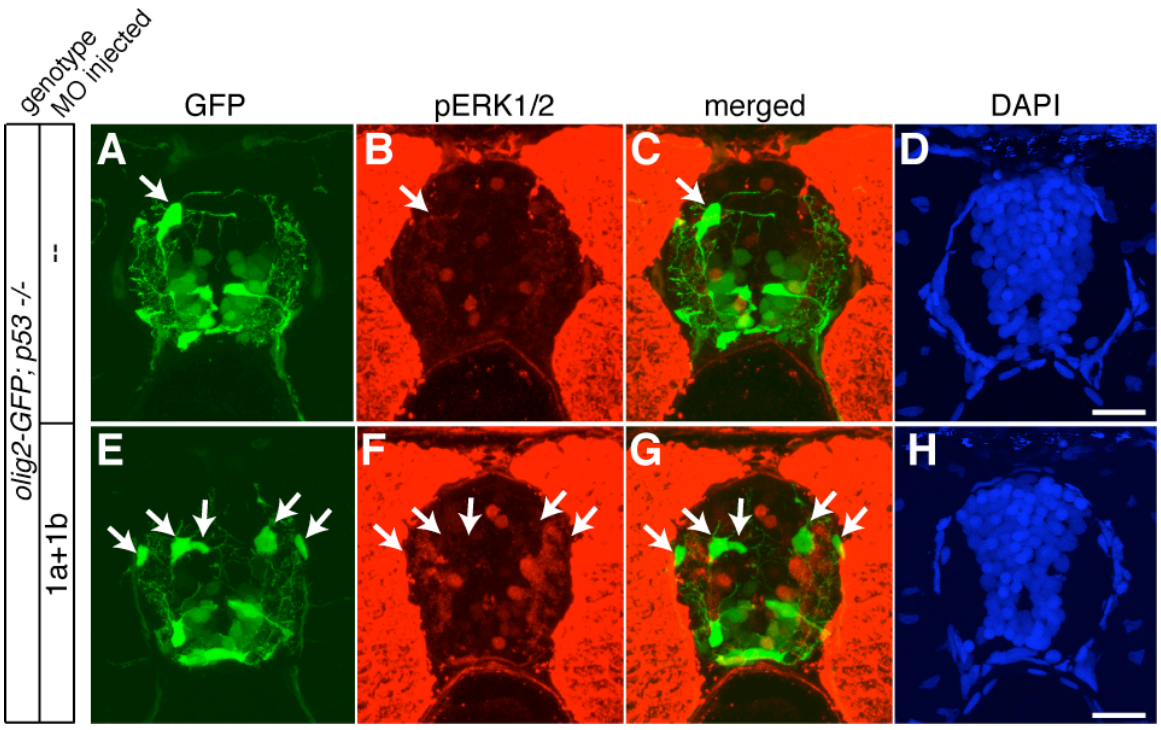

Fig. 6. Nf1 loss activates the RAS/MAPK pathway in the spinal cord, but not in OPCs.
Projected confocal images of transverse spinal cord sections labeled with GFP-(green) and phopho-ERK1/2-specific (red) antibodies. **(A-D)** An uninjected *olig2-EGFP*;*p53-/-* control embryo. **(E-H)** *olig2-EGFP*;*p53-/-* embryo injected with *nf1a* and *nf1b* morpholinos. Both the intensity of phospho-Erk1/2 staining and the number of phospho-Erk1/2-positive cells are increased upon nf1 loss; however, migrating GFP+ OPC cells in the dorsal spinal cord do not exhibit phospho-ERK1/2-labeling (arrows). Blue DAPI staining indicates cell nuclei (D, H).

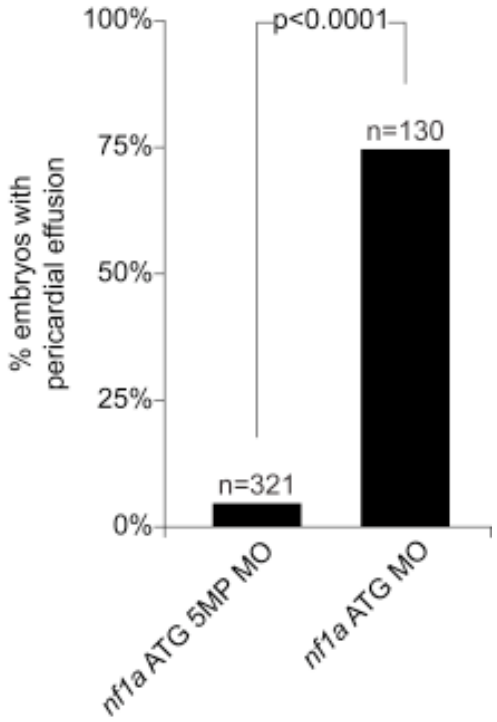

Fig. 7. MO knockdown of *nf1a* results in gross defects of cardiovascular development. Quantification of cardiovascular defects in 72 hpf *nf1a* ATG MO- and *nf1a* ATG 5MP MO-injected (2ng) embryos.

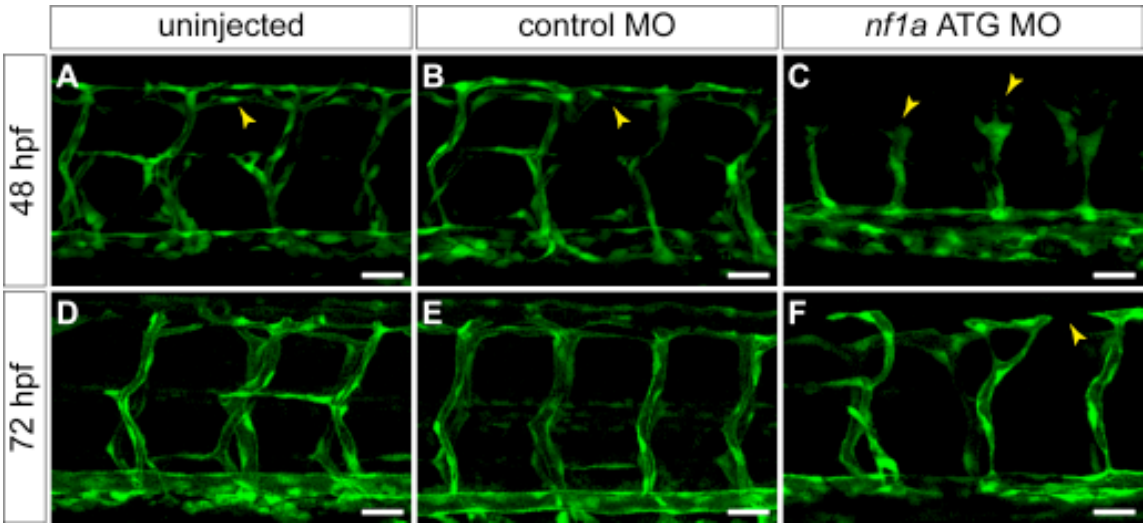

Fig. 8. **MO knockdown of *nf1a* results in vascular patterning defects at 48 and 72 hpf.** (**A-C**) At 48 hpf, *nf1a* ATG MO treated Tg(fli:egfp)y1 (endothelial-specific GFP transgenic) zebrafish embryos display gross defects in vascular development as compared with control MO treated or uninjected samples. Morphant embryos (**C**) display abnormal projections at the leading edge of the developing intersomitic vessels and fail to develop the dorsal longitudinal anastomotic vessel (DLAV) present in both controls MO treated (**B**) and uninjected (**A**) samples (arrows). (**D-F**) At 72 hpf, *nf1a* ATG morphant embryos display only rudimentary DLAVs (arrow) and disorganization of the vasculature (**F**) when compared with control MO treated (**E**) or uninjected (**D**) embryos. Scale bars: 25μm.

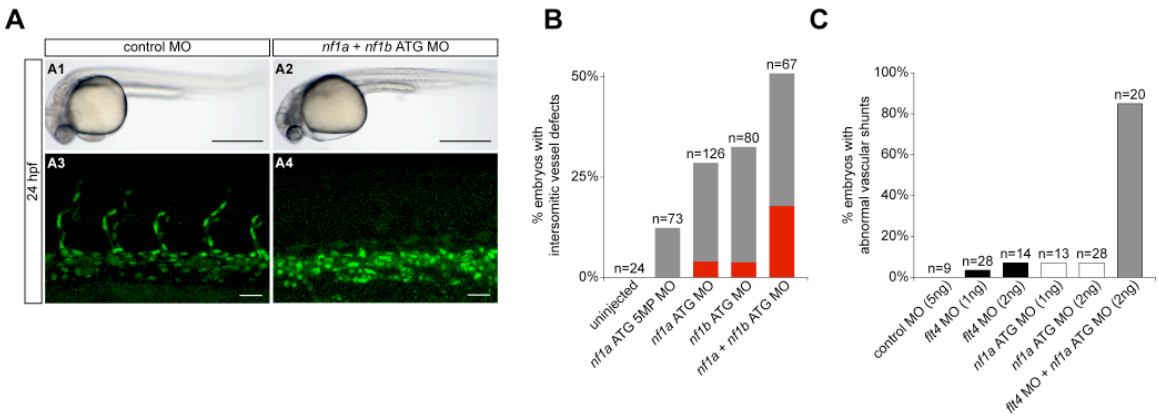

Fig. 9. **MO knockdown of *nf1a, nf1b*, or both result in vascular defects at 24 hpf.**
(**A, B**) Analysis and quantification of vascular defects at 24 hpf in uninjected and morphant Tg(fli:negfp)y7 (endothelial-specific nuclear GFP transgenic) zebrafish embryos. Control MO-treated (**A1**) and combined *nf1a*/*nf1b* MO-treated (**A2**) zebrafish embryos appear similar by gross morphological analysis at 24 hpf (scale bars: 500µm). Development of intersomitic vessels is deficient at 24 hpf in *nf1a*/*nf1b* combined morphants (**A4**) when compared to control MO-treated embryos (**A3**) (scale bars: 25µm). **(B)** Intersomitic vessel formation between somites 17-30 at 24 hpf was scored as absent (red), intermediate (grey) or normal (*nf1a* ATG 5MP MO refers to a control MO with 5 mispairs when compared to the *nf1a* ATG MO). (**C**) MO-mediated knockdown of *flt4*, providing a sensitized background for the detection of vascular defects, was combined with *nf1a* ATG MO knockdown. 85% of combined *flt4*/*nf1a* MO-treated embryos display abnormal vasculature as compared with 4-8% of individual *flt4* or *nf1a* MO-treated embryos.

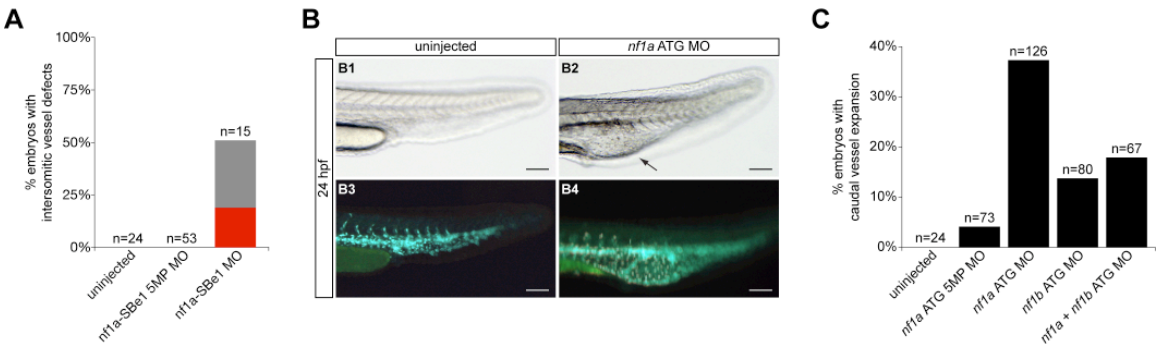

Fig. 10. MO knockdown of *nf1a, nf1b,* or both together result in vascular defects at 24 at 48 hpf. (A) Quantification of vasculature at 24 hpf in uninjected and morphant Tg(fli:negfp)y7 (endothelial-specific nuclear GFP transgenic) zebrafish embryos. *nf1a* morphant embryos were qualitatively assessed for presence, absence (red), or an intermediate phenotype (grey) with regard to the developing trunk intersomitic vessels between somites 17-30 at 24 hpf. (B1-B4) Treatment of Tg(fli:negfp)y7 zebrafish embryos with an *nf1a* ATG MO also leads to a cystic expansion in the region of the caudal artery and vein (B2) not present in uninjected embryos (B1) (scale bars represent 100µm). The expanded tissue was confirmed to be vascular by GFP expression (B3, B4) (scale bars represent 100µm). (C) This phenotype is present in *nf1a* ATG, *nf1b* ATG, and *nf1a*/*nf1b* combined ATG MOs as quantified.

A

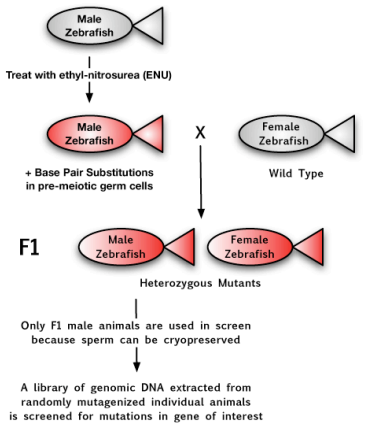

B

Nf1a	exon	mutation	Amino acid change
1 (M82)	Exon21	A**C**G→A**T**G	Thr→Met
2 (F211)	Exon21	C**C**G→C**T**G	Pro→Lys
3 (dir. seq.)	Exon26	CA**G**→CA**C**	Gln→His
4 (74-11)	Exon26	**T**CA→**C**CA	Ser→Pro
5 (VU180)	Exon26	A**T**G→A**A**G	Met→Lys
6 (T203)	Exon26	T**T**G→T**A**G	Leu→stop
Nf1b	**exon**	**mutation**	**Amino acid change**
zm-00346420	intron between Exon1 and Exon2	insertion	N/A

Fig. 11. Searching for zebrafish mutants for *nf1a* and *nf1b*
(A) Schematic of TILLING procedure. **(B)** A list of the mutations for *nf1a* and *nf1b* identified from TILLING thus far.

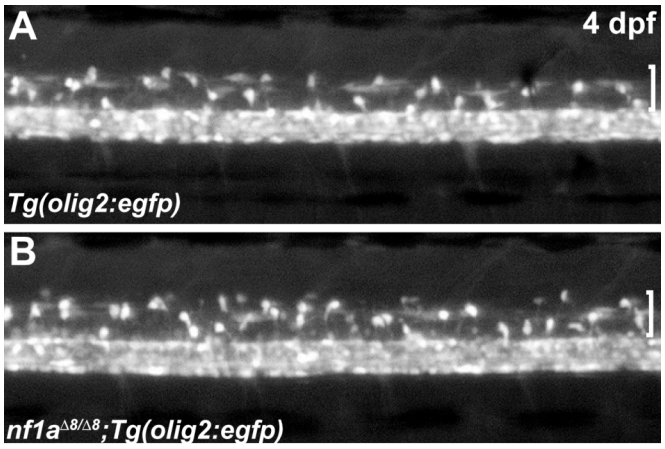

Fig. 12. OPC phenotype is recapitulated in *nf1a* mutant zebrafish line generated using engineered Zinc Finger Nucleases.
Increased number of GFP^{+} OLCs in *nf1a*$^{D8/D8}$;*Tg(olig2:gfp)* mutant embryos **(B)** when compared to wild-type **(A)** or heterozygous *nf1a*^{D8} embryos.

Key research accomplishments:

- Characterization of zebrafish orthologs: *nf1a* and *nf1b*.
- Analysis of gene expression of *nf1a* and *nf1b.*
- Analysis of morpholino knockdown phenotypes for *nf1a* and *nf1b*.
- Identification of fish with mutations in *nf1a* and *nf1b* via TILLING and through the use of engineered Zinc Finger Nucleases.
- Obtained and began breeding fish with insertional mutation in *nf1b*.

Reportable outcomes:
Two manuscripts describing the results obtained so far have been submitted for publication and are presently being revised to address reviewers' concerns.

Conclusion:
In this second year of study, we have furthered our advances towards meeting the goals set forth in the funded proposal. The target genes have been clearly identified and phenotypes due to morpholino knockdown have been characterized that are relevant to the understanding of human disease. While morpholino knockdown is informative, future experiments will be aided by the characterization of stable mutations within these genes in zebrafish. Significant strides have been made towards obtaining these mutant fish lines. Several different approaches have been undertaken which may result in an allelic series of mutant fish appropriate for further analysis throughout the scientific community. When characterized, these reagents will be freely shared with our colleagues. These reagents should be excellent candidates for use in screening small molecules and for use in performing genetic screens to identify modulators of this important disease.